Investigation of Flow field over Swept back Wing

[1]Samrat Biswas, [2]Animesh Roy, [3]Prabir Kr. De, [4]Bireswar Majumdar.
[1]PhD Research Fellow, [2] PhD Research Fellow, [3]Professor, [4]Professor
[1, 2, 4]Department of Power Engineering, Jadavpur University, Kolkata, India
[3]Department of Mechanical Engineering, Jadavpur University, Kolkata, India

Received: January 16, 2019 Accepted: March 03, 2019

ABSTRACT: *An experimental and numerical investigation with different angle of incidence (α) has been performed to study flow features over a swept-back wing, modeled after RAE 2822. The wing model was tested at Mach no. 0.04 between α range of 0° and 30°. Numerical study on this wing under similar conditions using one equation model of Spalart-Allmaras was also carried out. Aerodynamic parameters obtained using experiment and numerical methods were analyzed along-side. To further interpret the flow field a comprehensive series of surface flow visualization experimental data were also studied and compared with numerical surface streamlines data. The results showed increment in spanwise flow with increase in α. Change in aerodynamic parameters along with observable change in flow pattern over the surface is also noted. Results indicated formation and development of laminar separation bubble over wing leeward surface. Several different flow regimes laminar separation, separation bubble and 3D flow were observed.*

Key Words: : *Supercritical wing; swept-back wing; pseudo-stall phenomena; span-wise flow.*

Nomenclature

$AR =$	Aspect ratio
b	Span
C_A	Coefficient of axial force
C_D	Coefficient of drag
C_L	Coefficient of lift
C_M	Coefficient of pitching moment
C_N	Coefficient of normal force
C_r	Wing root chord
C_t	Wing tip chord
Exp	Experimental Value
M	Mach number
MAC	Mean aerodynamic chord
Num	Numerical Value
Re_{MAC}	Reynolds number using MAC
S	Planform area
α	Angle of attack (AoA)
Λ	Swept angle
λ	Taper ratio

I. Introduction

In late 1950s lot of experimental works has been carried out on swept-back wings in NASA. Among those literatures it has been found that Jones in 1947 (Jones, 1947) did a study on effects of sweepback on boundary layer and separation. It is now well-established that swept wing has greater critical Mach number than un-swept wing (Abbott & Von Doenhoff, 1959). The demand of cheap and safe high speed air travel became apparent post World War II in 1970s. This inspired research of newly designed wings for efficient performance at transonic or supersonic speeds. This eventually led to the development of the supercritical wing (NASA, 2018). Whitcomb developed the concept of supercritical wing (Wallace et al., 1998).

In 1970s AGARD was formed and under which series of experiments were carried out by aerodynamicists. Those experimental results were used later to validate numerical codes. Among those experiments Cook et. al. studied the two-dimensional configuration of RAE 2822 in 8-ft x 6ft transonic wind tunnel at Mach numbers ranging from 0.676 to 0.740 and chord based Re No. varied from $5.7x10^6$ to $2.7x10^6$. AoA was kept between 2.40° and 3.19°. Data included surface pressure measurements and mean flow boundary later and wake profiles deduced from traverse of pitot and static pressure measuring probes (Cook et al., 1979).

During late 1990s with advent of computation and steady progress in computation power brought many numerical methods and validation of experimental results using numerical methods. Slater (Slater, 1998) in 1998 demonstrated the computation results of flow over RAE 2822 airfoil section for two-dimensional turbulent, transonic flows about an airfoil. The study was validated using experimental results obtained from Cook et. al. (Cook et al., 1979). In 2000 Slater (Slater, 2000) did numerical study to verify the experimental results from the previously mentioned paper of Cook et. al. (Cook et al., 1979) at low Mach number 0.3 and zero AoA. Later in 2002 Slater (Slater, 2002) did numerical study of RAE 2822 transonic airfoil and validated results against the experimental data obtained from Cook et. al. (Cook et al., 1979). During the numerical study Spalart-Allmaras turbulence model (Spalart & Allmaras, 1994) was used to validate the results.

However the basic natures of most these experimental investigations are of confidential nature. Despite the obvious desirability of achieving a fundamental understanding of these low-speed phenomena problems most of the solutions for military aircrafts were reached in an empirical manner through wind-tunnel studies guided by only qualitative understanding of the phenomena involved. In more recent times development of small scaled aircrafts (e.g., UAV, MAV etc.) used for various purposes operate within large spectrum of Reynolds numbers span. These particular situations introduce the requirement of aerospace technological knowledge regarding low Reynolds number performance of airfoils.

Therefore, due to the interesting wider application of swept wings, it is considered of value to review the state of understanding in low-speed problems. Now-a-days aircrafts implement the super-critical airfoils to achieve acceptable transonic behavior. The purpose of this investigation is to access the behavior of flow field around the swept-back tapered wing configuration during take-off, landing and maneuvering or operation during low Reynolds number operation.

II . Experimental Facility

Schematic diagram in Figure 1 shows of an open loop suction type subsonic wind tunnel used to conduct the present investigation. Low turbulence wind tunnel of test section of 0.6 m×0.6 m located at Fluid Mechanics and M/C Laboratory, Dept. of Power Engineering, Jadavpur University is used. Test section has transparent windows on top and side walls to facilitate flow visualization studies. The free-stream velocity (u_∞) was measured with help of Pitot-static tube. Streamline Flow was achieved with the help of multiple turbulence screens and honeycomb structure installed upstream of 9:1 contraction cone, helping to produce free-stream turbulence intensity of less than 0.1%. Average velocity non-uniformity across the cross section was less than 0.5%.

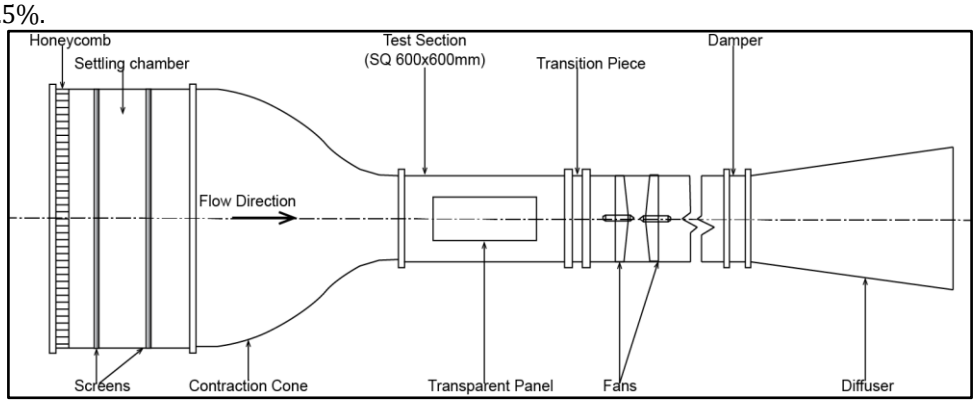

Figure 1: Schematics diagram of wind tunnel.

For present investigation tailless wing model of 30° swept back of RAE 2822 is considered for the investigation. Geometry of airfoil is made available from UIUC applied aerodynamics group (Selig, 2018). Details regarding geometry of the wing model are given in Table 1. Plan form view of wing model is given in Figure 2.

The entire set of experiment is carried out at a free- stream velocity of 12m/s at Re_{MAC} of 5.95×10^4. Lift, drag and moment were measured using a flat plate type 3-component strain gauge balance. A two axis model positioning system with motorized movement of α pitch angle, ranging from -10° to +30° is used. The mounting assembly is positioned outside of test section with suitable footings. It was also ensured that when the sector is at 0° of pitch, it coincides with the tunnel central axis. Data was recorded in between of 0° and 30° angle of attack. Aerodynamic forces and its coefficients were calculated using balance recorded raw data with the help of in-house written numerical code.

To facilitate visualization of flow structure over wing surface oil flow visualization technique was implemented. Ratio of the amount of oil, pigment and additive in oil-flow mixture and also the density of mixture was decided by several trial and errors. Wing is mounted on traversing mechanism with mixture applied on leeward surface, and is kept under experimental flow condition for certain amount of time for a flow pattern to be formed. Picture of these patterns is captured and recorded using digital camera. Captured images are used for qualitative and comparative analysis.

Table 1: Geometric Parameters of Wing

S	233.4784x10-4 m^2
$AR =$	4
b	0.3056 m
Λ	30°
λ	0.6
C_r	0.0955 m
C_t	0.0573 m

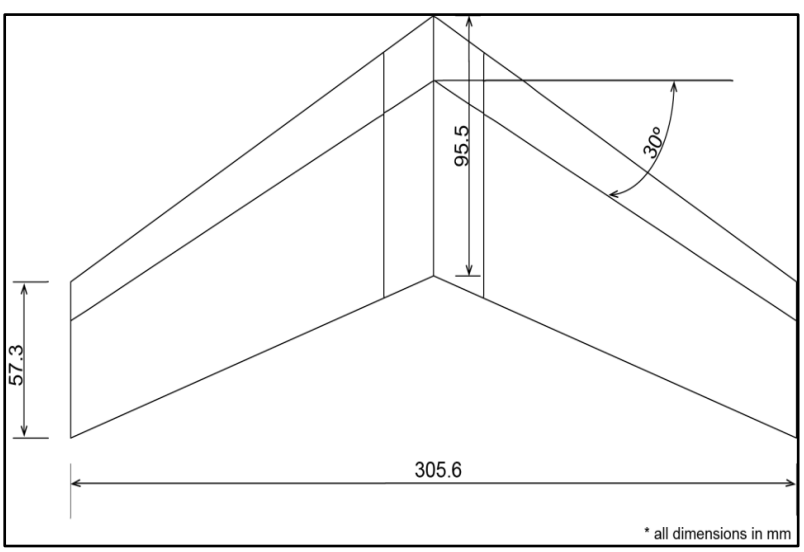

Figure 2: Geometry of the wing model.

III. Numerical Method

The wing model is also numerically simulated using an one-equation Spalart-Allmaras (SA) turbulence model. Spalart-Allmaras model was developed mainly for external flow over airfoil and wings (aerospace applications).

Geometry of the swept-back wing is created in CAD modeling software. Un-structured hybrid mesh grids are generated using Ansys ICEM CFD, which are combinations of tetrahedron, wedge and pyramids meshing. Results obtained from different sized mesh sizes having different number of cells e.g., 156655, 183395, 320636, 694714 etc. for Re_{MAC} of 5.95×10^4 at $\alpha = 10°$ were compared with experimental data to ensure grid independence. It was decided to conduct further simulations using 320636 numbers of cells. Since the difference between results of C_L value obtained from numerical and experimental measurement were found to be negligible with further refinement of mesh sizes.

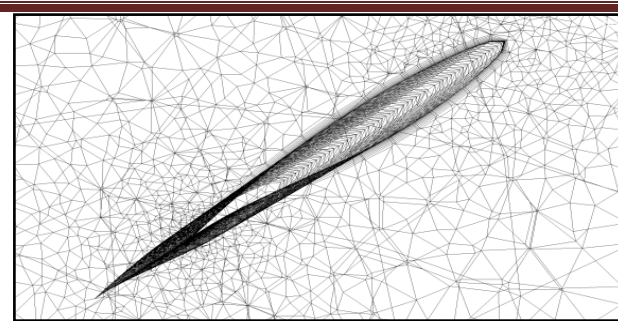

Figure 3: Cross-sectional view of the grid structure over wing.

Sectional view of the full mesh is shown in Figure 3. Near wall mesh sizes (average y^+ values of 1.5) are arranged appropriately to resolve the boundary velocity profile. Total 79008 numbers of nodes and 320636 numbers of elements are created in mesh. The mesh statistics are given in Table 2 and according to mesh quality criteria of ANSYS mesh quality improves significantly as value of orthogonal quality of mesh moves towards 1. Average mesh orthogonal quality found to be 0.83 for the present investigation. The mesh average skewness of the generated mesh has been maintained at 0.28. Density and viscosity are assumed for the prevailing flow without any significant change in temperature which in given in Table 3. Pressure-velocity coupling method with second order upwind spatial discretization scheme is used. Solution was initialized uniformly throughout the domain using free stream inlet condition. Velocity inlet with free stream velocity magnitude of 12 m/s is used as inlet boundary condition. No-slip wall condition is applied to the model surfaces. To simulate AoA, stream velocity directions are adjusted in accordance to required angle of attack. A convergence criteria of 10^{-3} is selected for the residuals. Various details like pressure, velocity, surface streamlines etc were obtained for comparison with experimental results.

Table 2: Mesh Statistics

mesh metric	minimum	maximum	average
orthogonal quality	2.45x10-002	0.99	0.83
skewness	1.12x10-003	0.98	0.28

Table 3: Parameters for Numerical Calculation

gas	air, ideal gas
density	1.177 kg/m3
viscosity	1.853e-05 kg/m-s
M	0.04
velocity	12 m/s
temperature	300 k

IV. Results and Discussion

4.1 Aerodynamic Parameters

Figure 4 shows profile plots of the lift coefficient (C_L), drag coefficient (C_D), and quarter chord moment coefficient (C_M), normal force coefficient (C_N) and axial force coefficient (C_A) which have been obtained experimentally for different AoA. Numerical results are also plotted against experimental results.

Figure 4(a) depicts the C_L rises with increase in AoA initially up to about 9° angle of attack. This gradually led to a point from where slope of curve starts to fall at about 15° AoA. This lift-fall phenomenon may be termed as "pseudo-stall". Numerical results also predict presence of "pseudo-stall" behavior along with experimental data characteristics at around the same location. Lift typically starts to fall when boundary layer transited from attached flow to separated flow. At about 19° angle of attack it is observed that C_L starts to increase again may be due to the appearance of turbulent flow over the wing. The lift rise phenomenon is induced from the reaction of the scavenging effect on the suction surface as observed by (Hoerner & Borst, 1975). It is known that "stalling" is used to specify C_L values where flow separation appears to have dominant effects on wing aerodynamic parameters. From this curve it can be conjectured logically that aerodynamic performances of a wing may be strongly affected by complex behavior of the boundary layer flow over the surface and also due to 3D flow structures originating from the end effects.

Figure 4(b) illustrates the distribution of C_D vs. α for the wing model. Figure 4(b) shows C_D increases with angle of attack α. The skin friction drag is a dominant factor in low angle of attack. And hence under close scrutiny it can be observed that rate of change in slope of curve changes slightly at around 10° angle of attack in resemblance with lift coefficient curve. After this change in slope the drag coefficient curve rises more sharply with increase in α. This figure also depicts that numerical results closely follow pattern of experimental results. This rise in the slope of curve expected to be the results of appearance of form drag along with the 3D flow effects over the wing.

Moment produced by aerodynamic forces on the swept wing model is measured against aerodynamic center of the model which is known as pitching moment. Figure 4(c) depicts the distribution of quarter-chord moment coefficient C_M obtained experimentally as well as numerically calculated values. The negative correlation between C_M and α indicates counter clockwise moment induced on the wing model. Here also it can be observed that slope of the C_M curves changes at around 10° AoA.

Up to around 20° AoA C_M decreases with the increase of α indicating appearance of "pseudo-stall". During 9°< α <14° increase in momentum C_M indicating less negative moment or increase in clockwise moment. For the region within 14°< α <20° C_M depicts steep-drop in curvature which indicates sudden loss of lift. For 20°< α <30° the curve shows downward behavior without presence of any drastic change in slope.

Figure 4(d) shows the variation of normal force with increase in angle of attack. It can be observed from Figure 4(d) that coefficient of normal force C_N increases maintaining upward slope up to about 9° of angle of attack. Further increase in angle of attack causes the change in slope of curve similar to lift coefficient as observed in Figure 4(a). Normal force curve observed to be changing its slope in accordance with lift coefficient, C_L curve slope characteristics. Property of normal force coefficient, C_N curve indicates normal component of the force contributes to C_L of wing.

Change of axial force coefficient C_A with respect to angle of attack is plotted in Figure 4(e). Similar to C_D for transition from attached flow to separation flow, there is a slight decrease in axial force, as flow gets influenced by span-wise component. But after at around 10° AoA 3D turbulence flow compensates for lost axial force to make the curve positive again.

Figure 4(f) depicts curve of drag coefficient, C_D with respect to the lift coefficient, C_L for wing model. The drag coefficient does not change significantly with increase of lift coefficient up to about C_L value of 0.6, but it is observed to increase steadily after C_L value reaches 0.6. The drag coefficient rises, while lift coefficient falls. After C_L value reaches 0.75, 3D turbulent flow region influence the drag coefficients to change again with variation in lift coefficient.

From Figure 4 this can be observed that calculated numerical value remains very close to experimental value. Numerical results even portray similar type of behavior like its experimental counterpart. It can be safely assumed that to further study of flow physics one can precede using numerical results.

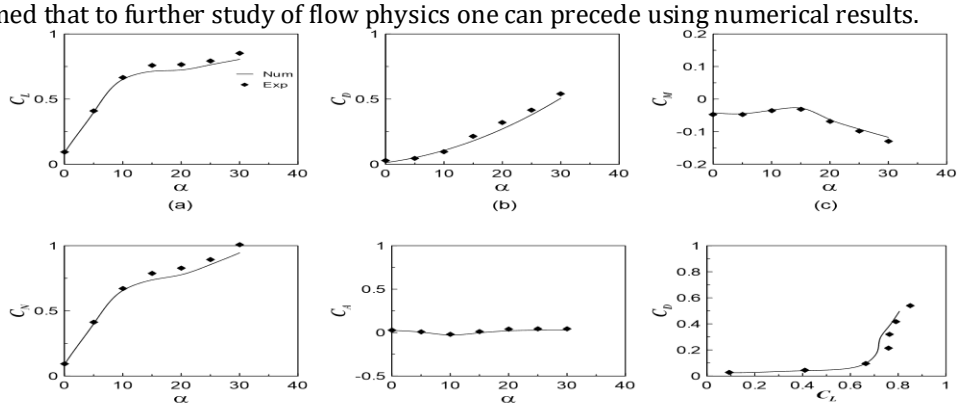

Figure 4: Aerodynamic parameters of swept-back wing: (a) Lift coefficient, (b) Drag coefficient, (c) Moment coefficient, (d) Normal force coefficient, (e) Axial force coefficient, (f) Drag coefficient vs. lift coefficient.

4.2 Surface Flow Visualization

Numerically computed and experimentally obtained surface flow patterns were plotted over the airfoil surface and is shown in Figure 5. For left half span of the wing model represent numerically calculated surface streamlines and right half span of wing model depicts experimentally obtained oil flow pattern. It illustrates surface flow pattern over leeward surface of RAE 2822 swept back wing model at AoA 0°, 10°, 15°, 20° at $Re_{MAC} = 5.95\times10^4$. It shows the effect of α on surface flow patterns. In Figure 5 deep black line with arrow delineates the schematic sketch of surface flow patterns in allusion with the surface flow pattern as shown in Figure 5. Numbers of surface streamlines have been reduced from Figure 5 and direction arrows are also added for further clarification. Lines formed in Figure 5 hint towards the positions of flow separation or reattachment. Flow patterns over the wing model were classified into several different flow conditions e.g., attached flow, laminar separation, separation bubble, extension of separation bubble, 3D flow etc. (Hoerner & Borst, 1975).

Figure 5(a) shows surface flow patterns at $\alpha = 0°$. Here it can be observed that the laminar boundary layer is attached on wing surface. The surface flow patterns move in mainstream direction starting from leading edge of the wing to trailing edge. The air flows smoothly over the wing surface in laminar fashion, therefore doesn't exist any traces of separation or vortical structures. This flow condition is identified as the attached flow condition.

Figure 5(b) indicates flow structures at incidence of 10°. Laminar Separation line is observed over wing surface. Span-wise flow affects heavily at this angle of attack as depicted by the Figure 5(b). The line shows the separation of flow along the spanwise direction of wing. The lines were distorted near middle portion and wingtip of the model due to end effects and similar case was discussed by Bertin and Smith (Bertin & Smith, 1989). At this flow condition a considerable portion of the boundary layer flow is 2D, except near to the wingtip. Over entire leeward surface of wing presence of heavy span-wise flow is observed. It can be observed that heavy span-wise flow push and distort surface streamlines or surface flow lines from root towards tip of wing.

The possible formation of laminar separation bubble, as artifact of low Reynolds number flow (Abbott & Von Doenhoff, 1959) can be observed at $\alpha = 15°$ which is shown in the Figure 5(c). The separation bubble appears from leading edge leaves impression of separation structure near trailing edge. Heavy span-wise flow pushes the flow lines from root towards tip and with increase in incidence angle effect of span-wise flow gets increased significantly.

Figure 5(d) and shows the flow structure at $\alpha = 20°$. The separation bubble seems to be present over the wing surface. Surface streamline near the root of the wing gets pushed towards root chord making more tight turn in comparison to surface streamline at $\alpha = 15°$ depicted in Figure 5(c).

The inboard flow at root stars from leading edge indicating formation of 3D flow and gets pushed towards tip of the wing. The outboard flow lines were from tip to root. Specifically in experimental part it can be observed that the flow lines indicate movement of flow towards the tip of the wing. Separated or stalled flow patterns are observed in the vicinity of wing tip portion. It can be deduced that as flow gets deflected from the leading edge forms a 3D vortex over the wing. With increase in angle of attack the 3D bubble over the wing gets pushed forward.

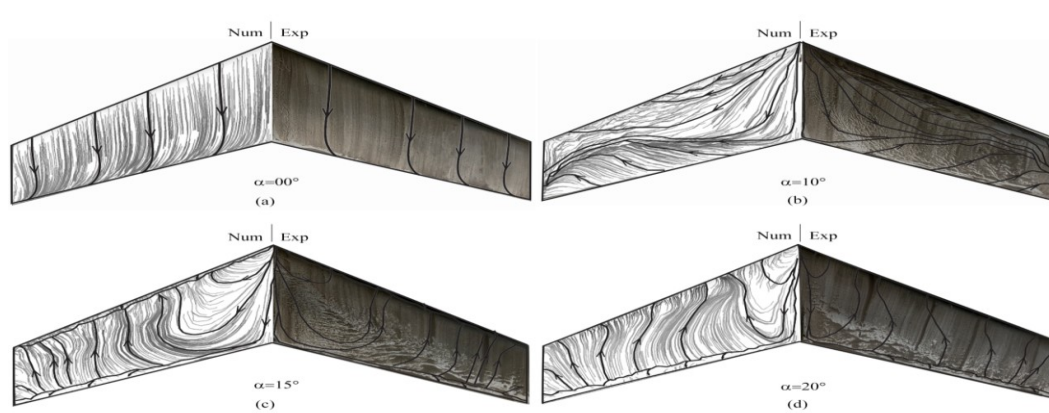

Figure 5: Surface Streamline flow pattern (oil flow).

V. Conclusion

From the present investigation the following conclusions can be drawn about tapered swept back wing model made using of RAE2822 supercritical airfoil profile operating under highly subsonic range. The aerodynamic performance of wing model between 0°< α <30° were investigated both experimentally and numerically. Characteristics boundary layer flow patterns were also studied using the experimental and numerically obtained results.

From experimental lift coefficient curve, it was observed that lift increases up about "pseudo-stall" then the lift decreases. After the "pseudo-stall" phenomena lift starts to increases again. Numerical model for turbulence suggested by Spalart-Allmaras (Spalart & Allmaras, 1994) calculates flow features and results bear close resemblance to the experimental counterparts.

After comparing experimental and numerical surface flow visualization, different boundary layer flow structures have been found to be formed over wing surface with change of α . Careful analyses of figures indicate different flow features like attached flow, laminar separation, separation bubble and 3D turbulent flow etc. was found. At 15° angle of attack it appears the size of the vortices starts to increase resulted in localized formation of separation bubble. With increase in angle of attack from 15° to 20° it was found that size of localized separation bubble get increase. It intended to more in depth study of the flow features over supercritical wing in subsonic region at different orientation.

Computational results showed overall good agreement with the experiment in context of aerodynamic parameters, surface flow visualization are well justified by Spalart-Allmaras turbulence model. Numerical results are found to vary on average within 12% of the experimentally obtained results.

References

1. Abbott, I. H., & Von Doenhoff, A. E. (1959). Theory of Wing Sections, including a summery of airfoil data. Courier Corporation.
2. Bertin, J. J., & Smith, M. L. (1989). Aerodynamics for Engineers (2nd Edition ed.). NJ: Prentice-Hall.
3. Cook, P. H., Mcdonald, M. A., & Firmin, M. C. (1979). Airfoil RAE 2822 - Pressure Distributions, and Boundary Layer and Wake Measurements, "Experimental Database FOr COmputer Program Assessment. NACA.
4. Hoerner, S. F., & Borst, H. V. (1975). Fluid-Dynamic Lift (second ed.). (H. V. Borst, Ed.) Brick Town, NJ, USA: Mrs. Liselotte A. Hoerner.
5. Jones, R. T. (1947). Effects Of SweepBack On Boundary Layer And Separation. NACA.
6. NASA. (2018). Retrieved from www.nasa.gov: https://www.nasa.gov/
7. Selig, M. (2018). Retrieved 2018, from UIUC Applied Aerodynamics Group, Department of Aerospace Engineering, University of Illinois : http://m-selig.ae.illinois.edu/ads/coord_database.html
8. Slater, J. W. (2000, January 7). NPARC Alliance CFD Verification and Validation. Retrieved from NPARC Alliance Validation Archive: https://www.grc.nasa.gov/www/wind/valid/raetaf/raetaf02/raetaf02.html
9. Slater, J. W. (2002, May 3). NPARC Alliance CFD Verification and Validation. (NASA) Retrieved from NPARC Alliance Validation Archive: https://www.grc.nasa.gov/www/wind/valid/raetaf/raetaf04/raetaf04.html
10. Slater, J. W. (1998, September 30). NPARC Alliance Validation Archive. (NASA, Producer) Retrieved from NPARC Alliance CFD Verification adn Validation: https://www.grc.nasa.gov/www/wind/valid/raetaf/raetaf01/raetaf01.html
11. Spalart, P. R., & Allmaras, S. R. (1994). A One Equation Turbulence Model for Aerodynamic Flows. La Recherche Aerpspatiale , 1, 5-24.
12. Wallace, Lane, E., & Mack, P. E. (1998). The Whitcomb Area Rule: NACA Aerodynamics Research and Innovation. From Engineering Science to Big Science. (P. E. Mack, Ed.) Washington, D.C.: University Press of the Pacific.